Journal of Structural Geology 33 (2011) 20–31

Contents lists available at ScienceDirect

Journal of Structural Geology

journal homepage: www.elsevier.com/locate/jsg

Application of the microboudin method to palaeodifferential stress analysis of deformed impure marbles from Syros, Greece: Implications for grain-size and calcite-twin palaeopiezometers

Toshiaki Masuda [a,*], Tomoya Miyake [a], Nozomi Kimura [b], Atsushi Okamoto [c]

[a] Institute of Geosciences, Shizuoka University, Shizuoka 422-8529, Japan
[b] Geological Survey of Japan, AIST, Tsukuba 305-8567, Japan
[c] Graduate School of Environmental Studies, Tohoku University, Sendai 980-8579, Japan

ARTICLE INFO

Article history:
Received 18 September 2009
Received in revised form
18 October 2010
Accepted 2 November 2010
Available online 13 November 2010

Keywords:
Calcite-twin palaeopiezometer
Differential stress
Grain-size palaeopiezometer
Marble
Microboudin method
Syros

ABSTRACT

Microboudinage structures developed within glaucophane are found in the calcite matrix of blueschist-facies impure marbles from Syros, Greece. The presence of these structures enables the successful application of the microboudin method for palaeodifferential stress analysis, which was originally developed for rocks with a quartzose matrix. Application of the microboudin method reveals that differential stress increased during exhumation of the marble; the estimated maximum palaeodifferential stress values are approximately 9–15 MPa, an order of magnitude lower than the values estimated using the calcite-twin palaeopiezometer. This discrepancy reflects the fact that the two methods assess differential stress at different stages in the deformation history. Differential stresses in the Syros samples estimated using three existing equations for grain-size palaeopiezometry show a high degree of scatter, and no reliable results were obtained by a comparison between the results of the microboudin method and grain-size palaeopiezometry.

1. Introduction

Microboudinage structures developed within columnar mineral grains such as amphibole, tourmaline, and epidote are common in quartzose tectonites within high-pressure/high-temperature metamorphic belts, and afford estimates of the magnitude of palaeodifferential stress when applying the microboudin method proposed by Masuda et al. (2003, 2008) and Kimura et al. (2006, 2010). This paper reports similar microboudinage structures, consisting of glaucophane embedded within a calcite matrix in two deformed impure marbles from Syros, Greece, and demonstrates that the microboudin method can be successfully applied to such marble tectonites.

Palaeodifferential stress analyses of marble can also be performed based on calcite twinning or the grain size of dynamically recrystallised calcite grains (e.g., van der Pluijm and Marshak, 2004; Passchier and Trouw, 2005). We applied the calcite-twin palaeopiezometer developed by Rowe and Rutter (1990) and the grain-size palaeopiezometer for calcite (Schmid et al., 1980; Rutter, 1995) to the analysed marble samples to compare the obtained palaeodifferential stress values among the three methods, which yielded contrasting results. We discuss how these values are compatible in terms of the differential stress history experienced by the marbles.

2. Samples of deformed marble

Microboudinage structures developed within glaucophane were found in two samples of impure marble collected as loose blocks (i.e., not in situ) from Kampos and Delfini in Syros, Greece (Fig. 1). The Delfini sample is the same as that described by Okamoto et al. (2006) in a study of chemical reactions during indentation at glaucophane–glaucophane contacts. The sampled marbles are part of the Cycladic blueschist–eclogite belt (e.g., Okrusch and Bröcker, 1990; Avigad and Garfunkel, 1991; Avigad et al., 1997; Trotet et al., 2001; Forster and Lister, 2005). They experienced blueschist–eclogite facies metamorphism during the Eocene (e.g., Maluski et al., 1987: Baldwin, 1996; Tomaschek et al., 2003; Forster and Lister, 2005). The peak temperature and pressure of the metamorphism were 450–520 °C and 1.2–2.0 GPa, respectively (Dixon, 1976; Dixon and Ridley, 1987; Okrusch and Bröcker, 1990; Bröcker and Enders, 1999). The samples show little evidence of a Miocene greenschist-facies overprint that has been well

* Corresponding author. Fax: +81 54 238 0491.
E-mail address: setmasu@ipc.shizuoka.ac.jp (T. Masuda).

0191-8141/$ – see front matter © 2010 Elsevier Ltd. All rights reserved.
doi:10.1016/j.jsg.2010.11.002

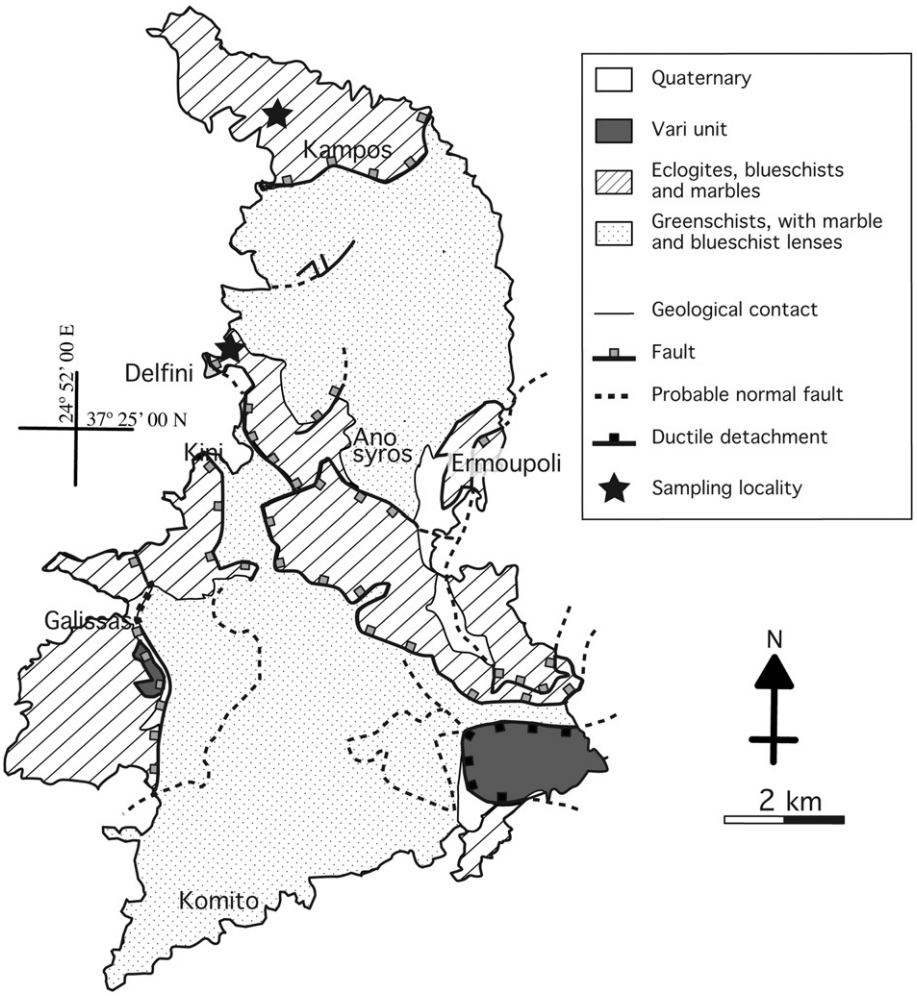

Fig. 1. Geological sketch map of Syros, modified after Trotet et al. (2001). The samples of deformed marbles analysed in the present study were collected at Kampos and Delfini.

established for the Cycladic area (e.g., Altherr et al., 1982; Lister et al., 1984). The samples are dominantly calcite (grain size, several tens of microns to >1 mm), with subordinate glaucophane, tourmaline, garnet, and muscovite. Calcite and glaucophane make up about 50% and 25% of the rock mass, respectively. The samples contain a clear foliation defined by aligned muscovite and glaucophane grains. No folding is apparent in the samples.

When viewing the foliation surface in thin section using an optical microscope, it is difficult to determine the mineral lineation visually (Fig. 2a). The mineral lineation was determined as the shape-preferred orientation of glaucophane, following the statistical method proposed by Masuda et al. (1999). We measured the angle between the long axis of the *i*th glaucophane grain and an arbitrarily drawn base line (θ_i), and a von Mises probability density function was applied to the results (Fig. 3) to determine the mean orientation ($\bar{\theta}$), the confidence interval (d_0), and the concentration parameter (κ). The lineation is then taken as the orientation of $\bar{\theta}$. The samples from Kampos and Delfini yielded κ values of 2.1 and 0.35, respectively. The distribution of long axes in the Kampos sample is narrower than that in the Delfini sample (Fig. 3).

3. Estimation of palaeodifferential stress using the microboudin method

The microboudin method of palaeodifferential stress analysis (Masuda et al., 1989, 1990) was originally inspired by the studies of Peter Misch, Colin C. Ferguson, and Geoffrey E. Lloyd, who presented beautiful examples of microboudins of chemically zoned amphibole (Misch, 1969, 1970), performed thoughtful strain analyses based on the boudins (Ferguson, 1981, 1985, 1987; Ferguson and Lloyd, 1984; Lloyd and Condliffe, 2003), demonstrated the difference in stress magnitude between that generated within boudins and that experienced by the surrounding matrix (Lloyd et al., 1982), and challenged existing methods of estimating palaeostress and strain (Ferguson and Lloyd, 1982). The microboudin method is also based on the Weibull statistics of the fracture strength of materials, especially the weakest-link theory (e.g., Weibull, 1951).

The method of palaeodifferential stress analysis performed using the microboudin technique was revised by Masuda et al. (2003), who incorporated the shear-lag model of Zhao and Ji (1997) into the model. Recent studies have advanced the microboudin method in the following four areas: (1) quantitative determination of the influence of the size of columnar minerals (Kimura et al., 2006, 2010), (2) consideration of the influence of time on the fracture strength of boudinaged minerals (Masuda et al., 2008), (3) experimental determination of the fracture strength of tourmaline and epidote (Kimura et al., 2006), and (4) determination of the fracture strength of amphibole (Kimura et al., 2010).

The microboudin method consists of two components: measurement of the length and width of microboudinaged and intact grains in metamorphic tectonites, and a theoretical analysis of fracturing. The analytical procedure is briefly described below. A full description of

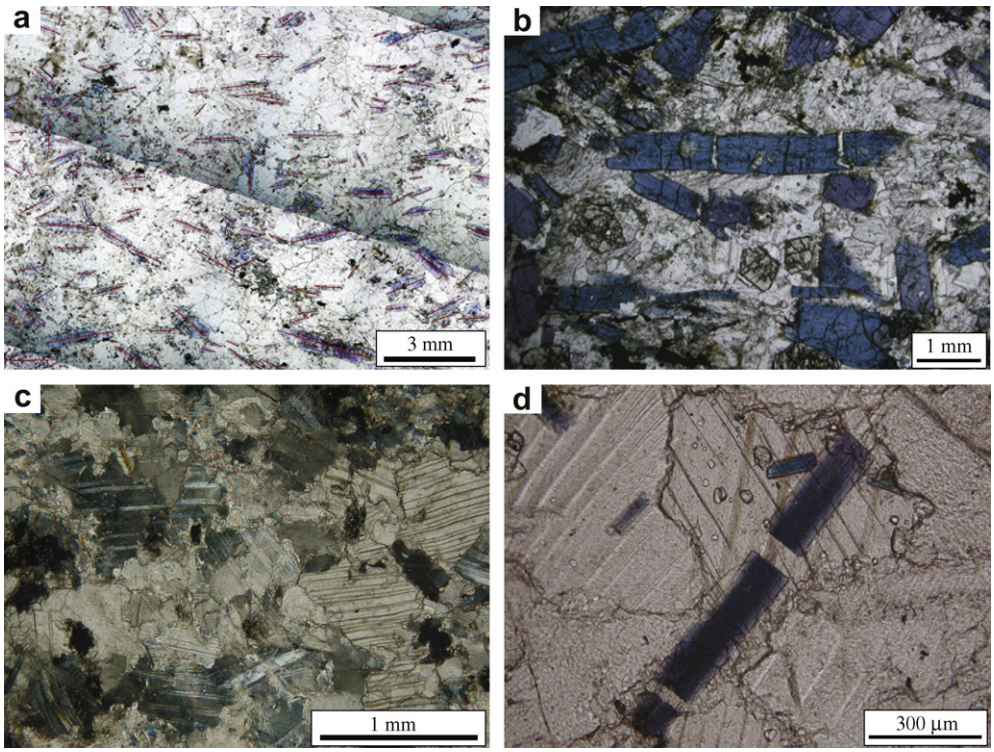

Fig. 2. Photomicrographs of deformed marble, viewed on the foliation surface. Green and purple grains are glaucophane, and transparent matrix grains are calcite. (a) Glaucophane grains (their long axes are indicated by red lines) within a calcite matrix in the Kampos sample. Plane polarised light. The straight boundaries across the photograph indicated by different colours are artifacts. (b) Glaucophane microboudins in the Delfini sample. Plane polarised light. (c) Calcite grains in the Kampos sample. Calcite grain boundaries range from straight through gently curving to slightly dentate. Thick, straight twins are prominent. Crossed polarised light. (d) Glaucophane microboudins surrounded by calcite grains. Thick twin lamellae (Type II) in the crystal are cut by thin twin lamellae (Type I). Thin and thick twin lamellae are unaffected at the interboudin gap of glaucophane microboudins. This observation demonstrates that calcite twinning occurred after the cessation of microboudinage. The lineation is parallel to the base of the photos for (a)–(c). The lineation in (d) is parallel to the long axis of glaucophane microboudins.

the mechanical and statistical aspects of the technique can be found in Masuda et al. (1989, 1990, 2003) and Kimura et al. (2010).

3.1. Observations of microboudinage of glaucophane

In the studied samples, the long axes of most glaucophane grains lie within the plane of the foliation. Fig. 2 shows photomicrographs of thin sections cut parallel to the foliation. Some columnar glaucophane grains are oriented at a high angle to the lineation (Fig. 3). Microboudinage structures are observed within columnar glaucophane grains in various orientations within the calcite matrix (Fig. 2b, d), which are fractured perpendicular to the long axis and pulled apart parallel to the long axis. The microboudins show no evidence of rotation relative to the lineation and foliation during microboudinage. According to the classification of boudins proposed by Goscombe et al. (2004), such microboudins of amphibole grains are classified as unmodified symmetric type, torn boudins group, blocky (object) boudins.

An electron probe microanalysis revealed that chemically zoned glaucophane grains were fractured and pulled apart during the microboudinage, and that actinolite overgrowths occur within interboudin gaps (Okamoto et al., 2006). These observations indicate that microboudinage occurred after glaucophane growth, during exhumation-related retrograde metamorphism.

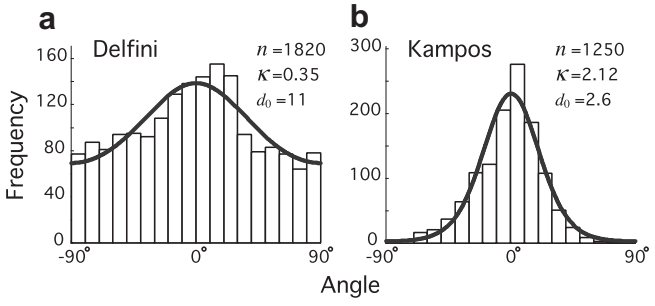

Fig. 3. Frequency distributions of the orientation of the long axes of glaucophane grains on the foliation surface. Fitting curves for the von Mises distribution are also shown (for details of this method, see Masuda et al., 1999). n is the total number of measured sodic amphibole grains, κ is the concentration parameter, and d_0 is the confidence interval for the critical region of 0.05. The distribution is arranged to set $\overline{\theta} = 0°$. $\overline{\theta}$ is the mean orientation.

3.2. Plastic deformation of calcite

Twinning of calcite is generally dealt with as a mechanism of plastic deformation (e.g., Passchier and Trouw, 2005), whereas in the present samples, calcite twinning occurred after the cessation of microboudinage (Fig. 2d). Thus, the plastic deformation of calcite during microboudinage occurred without any contribution by twinning. Because the major agents of plastic deformation are the movement of dislocations and the diffusion of atoms throughout the crystal lattice (e.g., Passchier and Trouw, 2005), we use the term 'diffusion–dislocation (D–D) plastic flow' to emphasise the occurrence of plastic deformation without calcite twinning and to prevent unnecessary confusion with 'plastic deformation'.

3.3. Reference frame of stress and strain

Given that the microboudins developed within glaucophane grains show no evidence of rotation relative to the lineation and

foliation, we assume that the strain field was coaxial and that the orientation of the principal stresses was constant during microboudinage: the maximum principal stress σ_1 was perpendicular to the foliation, and the minimum principal stress σ_3 was parallel to the lineation, upon the foliation surface (Fig. 4a). The magnitudes of the principal stresses are considered to have varied during microboudinage, without any change in the reference frame of stress and strain.

3.4. Basic equation

The far-field differential stress (σ_0) is given by Masuda et al. (2008) and Kimura et al. (2010) as

$$\sigma_0 = \lambda S_0^{**} \frac{K_0}{K_C} \left(\frac{1}{\overline{w}}\right)^{1/2}, \quad (1)$$

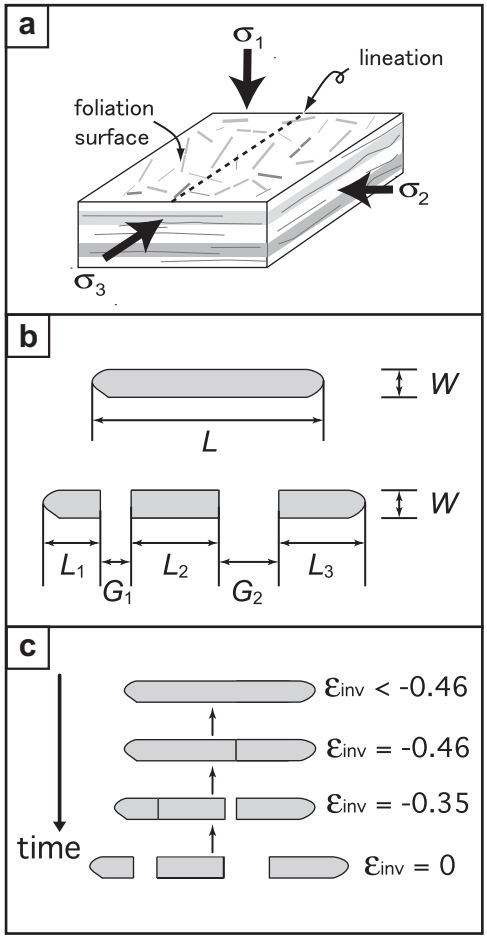

Fig. 4. Outline of the microboudin technique. (a) Assumed orientation of σ_1, σ_2 and σ_3 during the microboudinage event considered in this study. σ_1 is perpendicular to the foliation, σ_2 is perpendicular to the lineation within the plane of the foliation, and σ_3 is parallel to the lineation within the plane of the foliation. (b) Measurement of grain length (L, L_i), width (W), and interboudin-gap distance (G_i). (c) Example of the restoration of a microboudinaged grain using the strain reversal method of Ferguson (1981). In this example, a grain with an aspect ratio of 8.9 was fractured at $\varepsilon_{inv} = -0.46$, and a grain with an aspect ratio of 5.2 was fractured at $\varepsilon_{inv} = -0.35$. The fractured grains were subsequently pulled apart during microboudinage, until matrix flow ceased at $\varepsilon_{inv} = 0$. The aspect ratios of the three grains remaining at $\varepsilon_{inv} = 0$ are 2.1, 3.1, and 3.7. Thus, overall, we have one intact grain (aspect ratio = 8.9) at $\varepsilon_{inv} < -0.46$; one microboudinaged grain (aspect ratio = 8.9) and two intact grains (aspect ratios = 5.2 and 3.7) at $-0.46 \leq \varepsilon_{inv} < -0.35$; and two microboudinaged grains (aspect ratios = 8.9 and 5.2) and three intact grains (aspect ratios = 2.1, 3.1, and 3.7) at $-0.35 \leq \varepsilon_{inv} \leq 0$.

where λ is a dimensionless stress parameter, S_0^{**} is the instantaneous modal fracture strength of a 1 mm cube of amphibole, K_C is the fracture toughness, K_0 is the subcritical crack growth limit, and $\overline{w}$ is the mean width of glaucophane grains. This equation takes into account the influence of time (Masuda et al., 2008) and the size effect of fracture strength for glaucophane (Kimura et al., 2010). Among the parameters in Eq. (1), Kimura et al. (2010) determined that $S_0^{**} = 80$ MPa, while Kimura et al. (2010) tentatively proposed that $K_0/K_c = 0.1$. The value of K_0/K_c is assessed later. By substituting these values into Eq. (1), we have

$$\sigma_0 = 8\lambda \left(\frac{1}{\overline{w}}\right)^{1/2}. \quad (2)$$

Thus, an estimation of σ_0 requires λ and $\overline{w}$ to be determined. As λ and $\overline{w}$ are determined at any stage of the D–D plastic deformation of the bulk rock (see below), the microboudin method can be used to obtain differential stress–strain curves.

3.5. Geometric measurements of glaucophane grains

In this study, microboudinage analysis was only performed for glaucophane grains with long axes oriented within 15° of the mineral lineation upon the foliation surface. We measured the lengths, widths, and interboudin-gap distances of boudinaged glaucophane grains, as well as the lengths and widths of intact glaucophane grains (Fig. 4b). More than 500 boudinaged and intact grains were measured in the two samples. The frequency distributions of grain widths before microboudinage are shown in Fig. 5. Note that the total number of grains (intact grains and microboudins) increases with ongoing microboudinage (see Fig. 4c). The mean width $\overline{w}$ used in calculating σ_0 in Eq. (1) can be calculated at any stage of microboudinage development.

To restrict the analysis to D–D plastic flow, we exclude glaucophane microboudins with twinned interboudin-gap calcite grains from microboudinage analysis. We are only concerned with microboudinage related to D–D plastic strain.

3.6. Inverse natural strain

We used the strain reversal method (Ferguson, 1981, 1985, 1987; Ferguson and Lloyd, 1982, 1984; Lloyd and Condliffe, 2003) to calculate the D–D plastic strain recorded by each interboudin gap (Fig. 4c). The inverse natural strain (ε_{inv}) represents a quantitative measure of partial D–D plastic strain in the period between the time of fracturing and the time at which the matrix ceased to flow, with the origin of the strain ($\varepsilon_{inv} = 0$) corresponding to the latter time. As this time is considered to be synchronous for all microboudins in a rock mass, ε_{inv} can be used as a measure of the timing

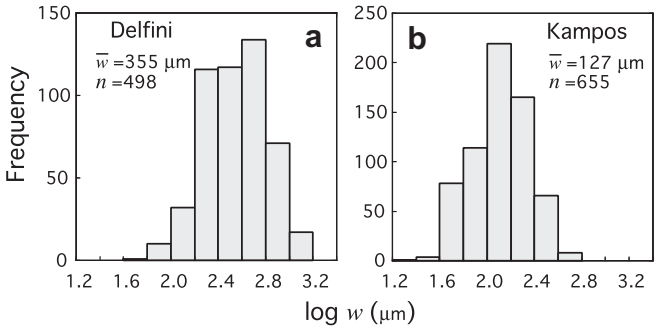

Fig. 5. Frequency distribution of the width of glaucophane grains at the pre-boudinage stage. The data are characterised by a log-Gaussian distribution. $\overline{w}$ is the geometric mean. n is the total number of measured grains.

of fracturing. The inverse natural strain is scaled toward the past and is given as a negative value.

Fig. 6 shows the aspect ratios of glaucophane grains within the Kampos and Delfini samples at the time of fracturing with respect to ε_{inv}, and the frequency distribution of fracturing with respect to ε_{inv}. The calculation was performed using a computer program developed by Masuda et al. (1994). The strain history of microboudinage differs between the two samples: the Kampos sample recorded >0.6 of D–D plastic strain during microboudinage, while the Delfini sample recorded only 0.2 of D–D plastic strain.

The frequency-distribution patterns of fracturing (Fig. 6) obtained for the two samples are characterised by a peak frequency at $\varepsilon_{inv} < 0$ and non-zero frequency at $\varepsilon_{inv} = 0$, indicating that fracturing took place immediately before the rocks ceased to flow. These frequency-distribution patterns correspond to Case C in the scheme proposed by Masuda et al. (2007), indicating that microboudinage occurred during exhumation-related retrograde metamorphism and that differential stress showed a progressive increase toward the end of D–D plastic deformation ($\varepsilon_{inv} = 0$).

3.7. Proportion of boudinaged grains

The proportion of boudinaged grains with respect to aspect ratio, which represents the most important data in differential stress analyses performed using the microboudin method, is defined as the ratio of the number of boudinaged grains to the total number of grains (boudinaged + intact) at each aspect ratio. Because the aspect ratio of fractured grains with respect to ε_{inv} can be calculated using the strain reversal method (Fig. 6), we reconstructed the frequency distributions of boudinaged and intact grains with respect to aspect ratio (r) at certain stages of microboudinage (see Fig. 7). Thus, the proportions of boudinaged grains at representative values of ε_{inv} are plotted in Fig. 8. The proportion of boudinaged grains is designated as $M(r)$, which appears in Eq. (4) below.

3.8. Stress parameter λ

Masuda et al. (2003) proposed a means of theoretically predicting the proportion of microboudinaged grains ($G(r, \lambda)$) as a function of the aspect ratio (r) of columnar grains and the stress parameter (λ), which was subsequently revised by Kimura et al. (2010) as follows:

$$G(r,\lambda) = 1 - \exp\left[-\frac{m-1}{m} r\lambda^m \left(\frac{E_f}{E_q}\right)^m \left\{1 - \left(1 - \frac{E_q}{E_f}\right)\frac{1}{\cosh(A_0 r)}\right\}^m\right], \quad (3)$$

where m is the Weibull modulus; E_f and E_q are the elastic constants of columnar grains and the matrix, respectively; and A_0 is a constant (for the derivation of Eq. (3), see Masuda et al., 2003). In the present case (i.e., columnar glaucophane grains within a calcite matrix), the constants E_f/E_q and A_0 have values of 1.4 and 0.5, respectively, following the data of Simmons and Wang (1971). Masuda et al. (2004) reported $m = 2$ for glaucophane.

The sum of the squared difference between $M(r_i)$ and $G(r_i,\lambda)$ is defined as a function of λ:

$$T(\lambda) = \sum_{i=1}^{N} h(r_i)[M(r_i) - G(r_i,\lambda)]^2, \quad (4)$$

where $h(r_i)$ is the total number of measured grains at each r_i; $M(r_i)$ and $G(r_i, \lambda)$ are $M(r)$ and $G(r, \lambda)$ for the measurement point (i), respectively; $r_i = i - 0.5$; and N is the number of measurement points. The value of λ is then determined to minimise $T(\lambda)$ with a weighting $h(r_i)$. This procedure is equivalent to obtaining the best-fit curve between $G(r_i, \lambda)$ and $M(r_i)$.

The standard deviation of the λ-value ($\Delta\lambda$) is calculated by

$$\Delta\lambda = \sqrt{\frac{1}{N-1}\frac{\sum_{i=1}^{N} h(r_i)[M(r_i) - G(r_i,\lambda)]^2}{\sum_{i=1}^{N} h(r_i)\left(\frac{\partial G(r_i,\lambda)}{\partial\lambda}\right)^2}}, \quad (5)$$

where

$$\frac{\partial G(r_i,\lambda)}{\partial\lambda} = -2C(r_i)\lambda\exp\left(C(r_i)\lambda^2\right) \quad (6)$$

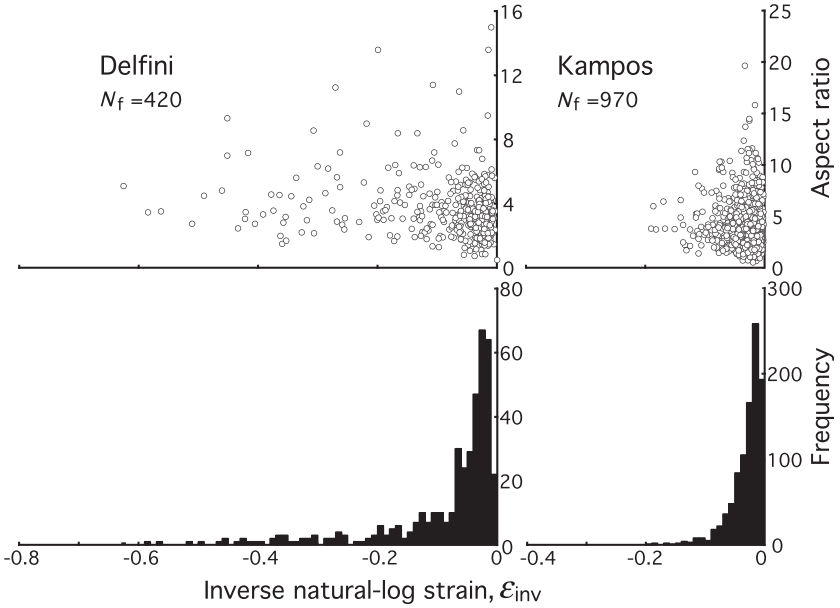

Fig. 6. Top: aspect ratios of fractured glaucophane grains with respect to inverse natural strain (ε_{inv}). Bottom: frequency distribution of fracturing events with respect to inverse natural strain (ε_{inv}). N_f is the total number of fracturing events.

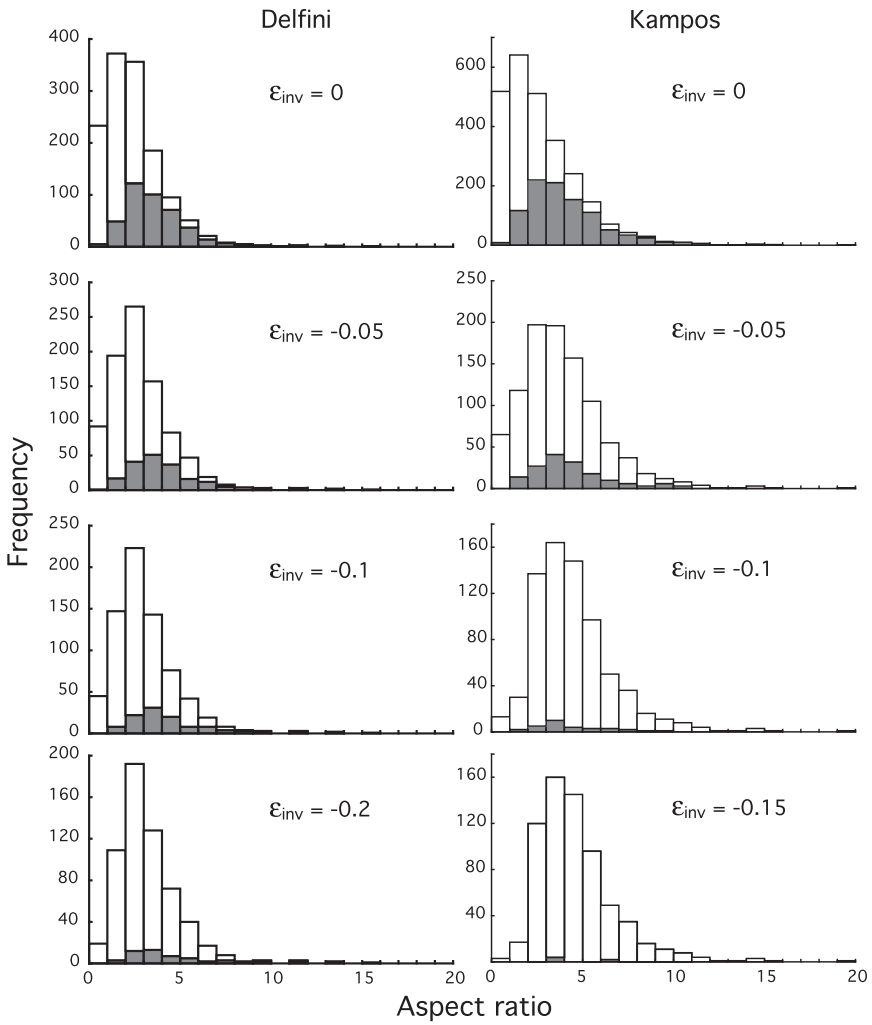

Fig. 7. Frequency distribution of the aspect ratios of microboudinaged (black bars) and intact (white bars) glaucophane grains with respect to aspect ratio at each ε_{inv}. These frequency distributions are representative. In this study, such frequency distributions are produced at every 0.01 of inverse natural strain (ε_{inv}) back to ε_{inv} of −0.62 and −0.20 for the Kampos and Delfini samples, respectively.

and

$$C(r_i) = -\frac{1}{2} r_i \left(\frac{E_f}{E_q}\right)^2 \left\{1 - \left(1 - \frac{E_q}{E_f}\right) \frac{1}{\cosh(Ar_i)}\right\}^2 \quad (7)$$

Fig. 8 shows the resultant λ- and $\Delta\lambda$-values and the best-fit $G(r, \lambda)$ at representative ε_{inv} for the Kampos and Delfini samples. The theoretical prediction $G(r, \lambda)$ shows an excellent fit to the measured data $M(r)$. This result strongly suggests that the microboudinage technique, originally developed for columnar minerals within quartzose tectonites, is also applicable to columnar minerals within marble tectonites.

The λ- and $\Delta\lambda$-values at each ε_{inv} can be obtained in the same way as that described above. $G(r, \lambda)$ also shows an excellent fit to $M(r)$ at each ε_{inv}.

3.9. Determination of σ_0

Above, we obtained the λ-value at each ε_{inv}. Using the strain reversal method, we also obtain $\overline{w}$ at each ε_{inv}. The values of $\overline{w}$ for the Kampos and Delfini samples at the pre-boudinage stage are 126 and 355 μm, respectively, while those at $\varepsilon_{inv} = 0$ are 126 and 412 μm, respectively. Substituting the obtained values of λ and $\overline{w}$ at each ε_{inv} into Eq. (2), we can determine σ_0 at each ε_{inv} (see Fig. 9).

3.10. Stress–strain curve

Fig. 9 shows that the values of σ_0 determined by the microboudin method for the Kampos and Delfini samples increase with increasing D–D plastic strain toward the end of D–D plastic strain at $\varepsilon_{inv} = 0$; the estimated σ_0 values at $\varepsilon_{inv} = 0$ for the Kampos and Delfini samples are 12 and 6.3 MPa, respectively. The differential stress–strain relationship is clearly different between the two samples: for the Kampos sample, the differential stress shows a gradual increase during the last >60% of D–D plastic strain, whereas for the Delfini sample it shows a relatively rapid increase during the last 20% of D–D plastic strain. These trends in differential stress reflect the fracturing history shown in Fig. 6. This contrast in differential stress–strain relations between the two samples clearly demonstrates that the state of stress is spatially heterogeneous, even within the same metamorphic terrain.

4. Grain-size technique for palaeodifferential stress analysis

Differential stress analysis based on the grain size of dynamically recrystallised grains was originally developed in the field of metallurgy (e.g., Sellars, 1978), and was applied to monomineralic

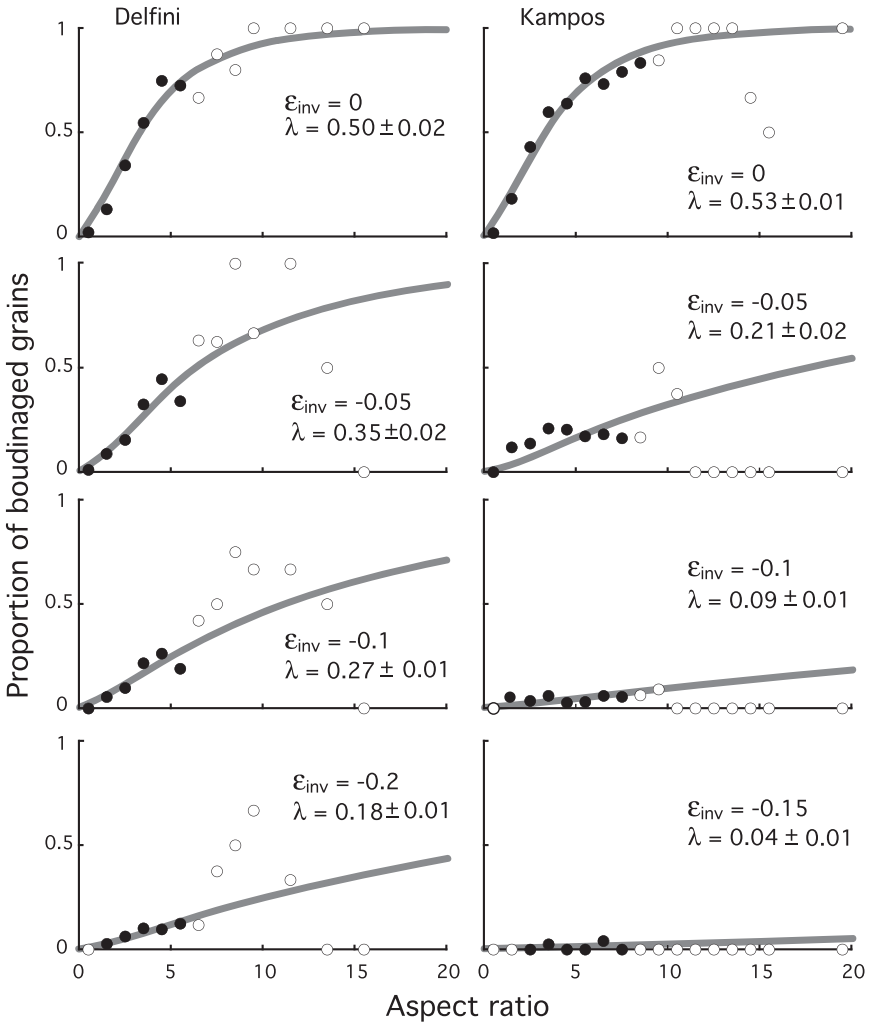

Fig. 8. Proportion of boudinaged grains (relative to the total number of grains) with respect to aspect ratio. Solid and open circles indicate reliable and less reliable data, respectively (>25 measured grains is regarded as reliable, while ≤25 measured grains is regarded as less reliable). Each curve represents the best-fit $G(r, \lambda)$ using all the data. The λ value at each ε_{inv} is indicated in each figure.

rocks in the mid-1970s (e.g., Mercier et al., 1977; Twiss, 1977). The basic equation relating differential stress to grain size has been empirically established based on the results of high-pressure and high-temperature deformation experiments (e.g., Schmid et al., 1980; Rutter, 1995; Shimizu, 2008; and many references therein). This method assumes steady-state flow; hence, a single differential stress value is given for each rock type. In the original grain-size palaeopiezometer developed by Twiss (1977) and Mercier et al.

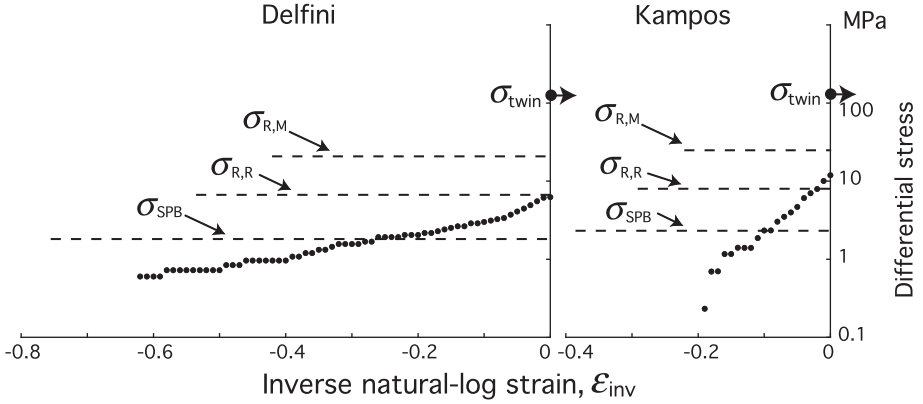

Fig. 9. Stress–strain histories determined using three different methods (microboudinage, calcite twin, and grain-size methods). The microboudin method only provides the change in differential stress (σ_0) with respect to ε_{inv}. The differential stress σ_{twin} was estimated using the calcite-twin palaeopiezometer of Rowe and Rutter (1990), while σ_{SPB} was estimated using the calcite grain-size palaeopiezometer of Schmid et al. (1980). The differential stresses $\sigma_{R,R}$ and $\sigma_{R,M}$ are those estimated using the equations proposed by Rutter (1995) for rotation recrystallisation and migration recrystallisation, respectively. σ_{SPB}, $\sigma_{R,R}$, and $\sigma_{R,M}$ are indicated by horizontal dashed lines irrespective of ε_{inv}, while σ_{twin} is indicated by arrowed points at $\varepsilon_{inv} = 0$ (the arrows indicate that the twinning occurred after the cessation of D–D plastic flow of calcite at $\varepsilon_{inv} = 0$).

(1977), differential stress is considered to be unaffected by the deformation temperature; however, the validity of this assumption has been questioned in a recent theoretical study (Shimizu, 2008).

Most palaeodifferential stress analyses of naturally deformed monomineralic tectonites using the grain-size technique focused on quartzose metamorphic tectonites (e.g., Kohlstead and Weathers, 1980; Etheridge and Wilkie, 1981; Ord and Christie, 1984), olivine-rich mantle rocks (e.g., Mercier, 1980), and marble mylonites (e.g., Pfiffner, 1982; De Bresser et al., 2002).

4.1. Basic equation

The magnitude of differential stress can be calculated by the following simple equations:

$$\sigma_{SPB} = \frac{467}{d^{1.01}}, \quad (8)$$

$$\sigma_{R,R} = \frac{813}{d^{0.88}}, \quad (9)$$

$$\sigma_{R,M} = \frac{2692}{d^{0.89}}, \quad (10)$$

where σ_{SPB}, $\sigma_{R,R}$ and $\sigma_{R,M}$ are differential stresses, and d is the grain size of dynamically recrystallised grains in microns (e.g., Schmid et al., 1980; Rutter, 1995; De Bresser et al., 2002; van der Pluijm and Marshak, 2004). σ_{SPB} was experimentally determined by Schmid et al. (1980), whereas $\sigma_{R,R}$ and $\sigma_{R,M}$ were experimentally determined by Rutter (1995) for rotation recrystallisation and for migration recrystallisation, respectively. Thus, σ_{SPB}, $\sigma_{R,R}$, and $\sigma_{R,M}$ can be calculated using these equations if grain-size d is known.

4.2. Observations of calcite grains

Fig. 2c and d shows photomicrographs of microstructures within calcite grains. The geometries of grain boundaries range from straight to gently curving and slightly dentate. Small calcite grains sometimes occur within interboudin gaps between glaucophane microboudins, while larger individual grains of calcite sometimes contain glaucophane microboudins.

These observations of calcite grains did not provide sufficient evidence to enable us to distinguish the mechanism of dynamic recrystallisation (i.e., rotation recrystallisation vs. the migration recrystallisation) by which these microstructures formed.

4.3. Measurements of grain-size

The boundaries of calcite grains within calcite-rich aggregates were carefully sketched on images of thin sections cut parallel to the foliation, and the sizes of the sketched grains were measured using image analysis software (NIH Image, http://rsb.info.nih.gov/nih-image/). Calcite grains within interboudin gaps were not measured. Grain size is defined as the diameter of a circle with the same area as that of the analysed grain. The grain sizes obtained for more than 450 grains in each sample are well fitted by a log-Gaussian distribution (Fig. 10), with geometric mean grain sizes $\overline{d}$ of 188 and 234 μm for the Kampos and Delfini samples, respectively.

4.4. Estimates of palaeodifferential stress

In this analysis, we assume $\overline{d} = d$. Using Eq. (8) of Schmid et al. (1980), we obtained palaeodifferential stress magnitudes σ_{SPB} for the Kampos and Delfini samples of 2.4 and 1.9 MPa, respectively. The values are shown as horizontal dashed lines in Fig. 9 because

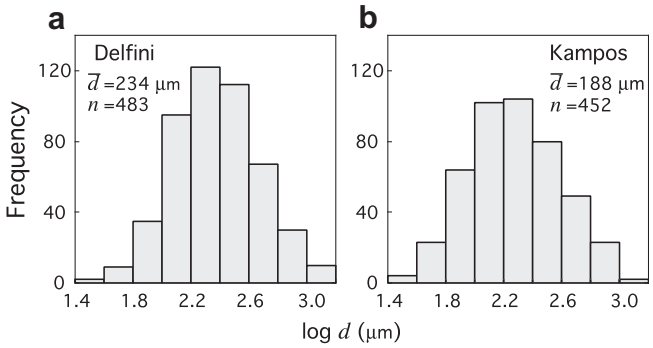

Fig. 10. Grain-size distributions of calcite. The data are well represented by log-Gaussian distributions. d is the grain size of calcite. n is the total number of measured grains. The geometric mean grain-size $\overline{d}$ was used for palaeodifferential stress analysis using grain-size palaeopiezometry.

they are largely independent of ε_{inv}. These values are between 1/4 and 1/6 of those determined by the microboudin method at $\varepsilon_{inv} = 0$, and are at least an order of magnitude higher than those determined by the microboudin technique at $\varepsilon_{inv} < -0.3$. Using Eqs. (9) and (10) proposed by Rutter (1995), the obtained values of differential stress $\sigma_{R,R}$ for rotation recrystallisation are 8.1 (Kampos) and 6.7 MPa (Delfini), whereas $\sigma_{R,M}$ for migration recrystallisation is 25 (Kampos) and 21 MPa (Delfini) (Fig. 9).

5. Calcite-twin technique

Calcite grains in both of the analysed samples contain ubiquitous twin lamellae (Fig. 2). Since the pioneering work of Turner (1953), several methods of stress analysis have been developed based on calcite twin data (e.g., Jamison and Spang, 1976; Laurent et al., 1990; Rowe and Rutter, 1990; Lacombe and Laurent, 1992, 1996; Burkhard, 1993; Lacombe, 2007). Many calcite-twin data have been accumulated from various tectonic environments using the techniques proposed by Jamison and Spang (1976) and Rowe and Rutter (1990) (e.g., Burkhard, 1993; Lacombe, 2007; and many references therein). Here, we apply the twin-density technique proposed by Rowe and Rutter (1990), because this technique is considered to be the simplest and most easily applied without the need to determine the orientation of calcite crystallographic axes with respect to the orientation of the principal stresses.

5.1. Basic equation

This method makes use of the twin density of calcite with respect to grain size. According to Rowe and Rutter (1990), the palaeodifferential stress σ_{twin} is empirically calculated by

$$\sigma_{twin} = -52.0 + 171.1 \times \log D, \quad (11)$$

where D is the twin density, defined as the rate of change in the number of lamellae of a given twin set with respect to grain diameter, measured normal to the trace of the twin lamellae. Twin density is expressed as the number of twins per millimeter distance. Eq. (11) indicates that σ_{twin} is directly calculated by determining D.

5.2. Observations of calcite twins

In terms of calcite twins within the analysed samples, thin and straight Type I twins (for a summary of twin types, see Burkhard, 1993; Passchier and Trouw, 2005) are ubiquitous, as are thick,

straight Type II twins; curved and sutured Type III and Type IV twins are absent. Because the incidence of twins appears to be dependent on grain size, the proportion of twinned grains is measured with respect to grain size (Fig. 11), revealing a higher proportion of twinned grains for larger sizes: all grains with a size of >300 μm are twinned. Thick type II twin lamellae are cut by thin Type I lamellae (Fig. 2d), demonstrating that the Type II twins predate the Type I twins.

A key observation in determining the relative timing of calcite twinning and microboudinage of glaucophane is whether calcite twins are present in the interboudin gaps between glaucophane microboudins. Fig. 2d shows Type I and Type II twin lamellae (Kampos sample) continuously developed throughout glaucophane microboudins and an interboudin gap. This observation indicates that the microboudins and the interboudin gap do not disturb the occurrence of the thin and thick twin lamellae, demonstrating in turn that the calcite twinning post-dates the microboudinage event. Given that microboudinage (i.e., D–D plastic flow of calcite) ceases at about 250 °C (e.g., Ferrill et al., 2004; Passchier and Trouw, 2005), the twinning is considered to have occurred at <250 °C, consistent with the temperatures estimated by Ferrill et al. (2004) for thin Type I twins (<170 °C) and thick Type II twins (>170 °C).

5.3. Determination of twin density

The combined density of Type I and Type II twins was measured in the same thin sections as those used for microboudinage analysis and grain-size analysis (Fig. 12), yielding an excellent least-squares fitting by the straight line from the origin. Thus, the twin density D, determined as the slope of the fitting line, is considered to be independent of grain size. The resulting D values for the Kampos and Delfini samples are 13.4 and 11.4 (number of twins per millimeter), respectively.

5.4. Palaeodifferential stress estimates

By substituting the obtained D values into Eq. (6), the magnitudes of σ_{twin} are estimated to be 141 and 129 MPa for the Kampos and Delfini samples, respectively. These palaeodifferential stress magnitudes are plotted as points (marked by arrows) at $\varepsilon_{\text{inv}} = 0$ in Fig. 9, because they correspond to certain stages in the deformation history that post-date $\varepsilon_{\text{inv}} = 0$, when the rocks passed out of the D–D plastic flow regime. These differential stress values are about an order of magnitude higher than the estimated values at $\varepsilon_{\text{inv}} = 0$ obtained using the microboudinage technique, and between 5 and >10 times higher than those obtained using the grain-size method.

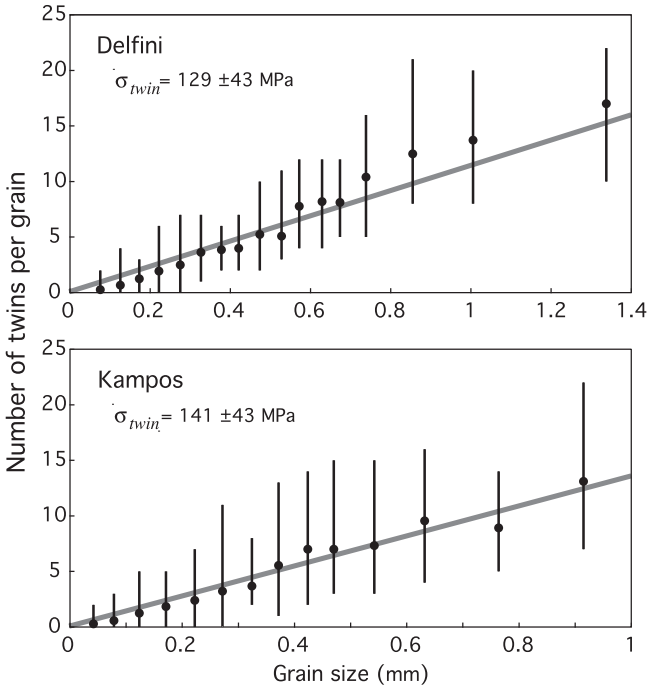

Fig. 12. Number of twins per grain with respect to grain size. The slope of the least-squares regression line from the origin represents the twin density.

6. Discussion

Our analysis of the two samples collected from Syros represents the first opportunity to compare the palaeodifferential stress magnitudes estimated using three different palaeopiezometric methods. As evident in Fig. 9, the three sets of estimates are apparently incongruent. The microboudin method provides differential stress magnitudes as a function of the D–D plastic strain of calcite, whereas the calcite twin and grain-size palaeopiezometers yield just a single differential stress value for each sample. Before evaluating the stress data obtained using the three methods, we first briefly compare the advantages and disadvantages of each technique.

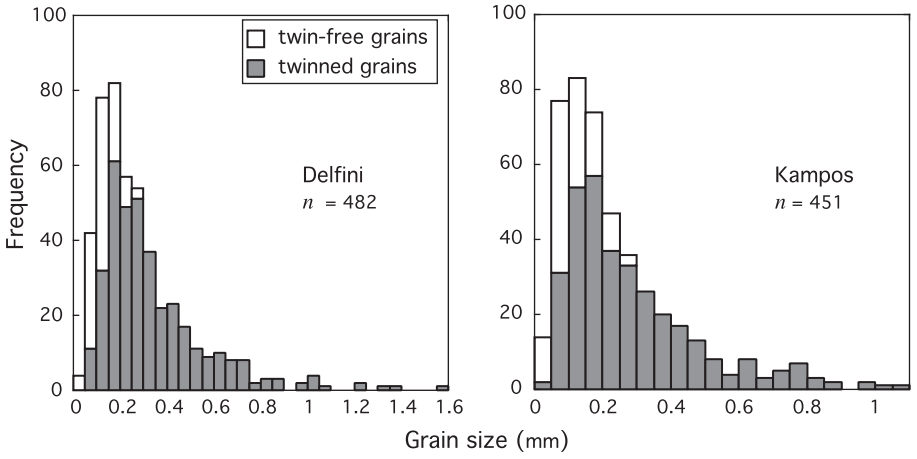

Fig. 11. Basic data employed in the analysis by calcite-twin palaeopiezometer.

6.1. Microboudin technique

We emphasise again that microboudinage structures embedded within a calcite matrix can be successfully analysed using the microboudin method, which was originally developed for rocks with a quartzose matrix. The microboudin method is considered the most informative among the three techniques employed here, because it can trace the trend in differential stress with increasing D–D plastic strain (Fig. 9). The general trend of increasing differential stress with increasing D–D plastic strain is considered reliable because the frequency distribution of fracturing with respect to inverse natural strain, as observed in the present study (Fig. 6), corresponds to Case C of Masuda et al. (2007), thereby providing evidence of increasing differential stress with increasing D–D plastic strain until the cessation of D–D plastic strain in matrix minerals.

The magnitude of differential stress estimated using the microboudin method is subject to revision, as the method is based on several unverified assumptions. For example, it is assumed that the value of S_0^{**} (= 80 MPa) is independent of temperature, pressure, and strain rate, and that $K_0/K_c = 0.1$. To improve the reliability of estimates of palaeodifferential stress based on the microboudin technique, it is necessary to evaluate the validity of these assumptions. Later, after synthesising the stress data obtained from the microboudinage and calcite-twin techniques, we present supporting data for $K_0/K_c = 0.1$.

6.2. Grain size palaeopiezometry

An advantage of the grain-size method is the ease with which palaeodifferential stress can be quantified, as this method only requires the measurement of grain sizes under a standard optical microscope, without the need for specialised techniques or electronic equipment such as TEM or EBSD (e.g., Passchier and Trouw, 2005). Many researchers, attracted by its ease of application, have used this method to estimate palaeodifferential stress from various tectonic settings (e.g., Kohlstead and Weathers, 1980; Mercier, 1980; Etheridge and Wilkie, 1981; Pfiffner, 1982; Ord and Christie, 1984; De Bresser et al., 2002). However, this method has three weaknesses: (1) theoretical ambiguity regarding its independence of temperature, (2) difficulty in extrapolating experimental strain rates to natural strain rates, and (3) the invalid assumption of steady-state flow during natural deformation.

Shimizu (2008) discussed the problem of temperature independence, and proposed a new equation for estimating palaeodifferential stress for quartz, demonstrating that palaeodifferential stress is a function of grain size and temperature. Unfortunately, the author did not produce a similar equation for calcite; however, it is reasonable to expect that the equation for calcite would be dependent on temperature. Thus, Eq. (5) is subject to revision.

The second problem lies in the difference between experimental and natural strain rates. Eq. (5) is empirically derived from the results of high-pressure/high-temperature deformation experiments. By necessity, experimental deformation occurs at much higher strain rates ($\sim 10^{-3}$–10^{-7} s^{-1}) than those of natural deformation ($\sim 10^{-13}$–10^{-16} s^{-1}). It remains unclear how to assess the influence of strain rate in terms of evaluating the reliability of this method when applied to natural deformation.

Finally, the grain-size method assumes steady-state microstructures produced by steady-state flow, where steady-state microstructures are defined as apparently unchangeable microstructures produced by deformation at a constant pressure, temperature, strain rate, and differential stress with increasing strain or time. Thus, it is only possible to produce such microstructures in experimentally deforming samples under controlled conditions. Steady-state flow is unlikely to occur in natural deformation because deformation conditions are uncontrollable: pressure and temperature show temporal and spatial variations during prograde and retrograde metamorphism, and differential stress is expected to vary over the course of the deformation history. An example of such variation is the differential stress–strain data shown in Fig. 9, as obtained using the microboudin method. Thus, calcite microstructures in naturally deformed marbles observed in the laboratory are never steady-state microstructures, but are the products of complex processes that occurred under various conditions of pressure, temperature, stress, and strain. Differential stress magnitudes based on the concept of steady-state flow are always problematic when applied to natural deformation.

6.3. Calcite-twin palaeopiezometry

An advantage of the calcite-twin method proposed by Rowe and Rutter (1990) is the ease in obtaining twin data, whereas a disadvantage is the difficulty involved in evaluating the obtained stress data in relation to the deformation history, as this method provides just a single differential stress magnitude for each sample. This advantage and disadvantage are shared with the grain-size method, but the calcite-twin method is more practical because it does not assume the steady-state flow of calcite.

Previous studies have argued that the method proposed by Rowe and Rutter (1990) leads to overestimates of differential stress (e.g., Burkhard, 1993; Ferrill, 1998; Lacombe, 2007); accordingly, the differential stress values obtained for the Kampos and Delfini samples in the present study may also be overestimated. According to Burkhard (1993), in the case that the local shear stress exceeds the critical resolved shear stress for calcite twinning (about 10 MPa), twinning should be related to strain magnitude rather than stress magnitude. Thus, even under a constant far-field differential stress, the number of calcite twins will increase with increasing strain. This results in overestimated stress values.

7. Implications for the use of palaeopiezometers

As stated above, each of the three considered palaeopiezometers has its limitations. In the following points, we discuss the applicability of the three methods and reconstruct the differential stress history of the analysed samples.

(1) In comparing the results of microboudin analysis with the calcite twin analysis, the obtained σ_{twin} values are higher than σ_0 at $\varepsilon_{inv} = 0$ for both samples (Fig. 9). This finding suggests that differential stress increased continuously from the initiation of microboudinage, through the point at which D–D plastic flow ceased, to the stage of calcite twinning, as shown schematically in Fig. 13. Differential stress is considered to have decreased after the termination of calcite twinning, when the sampled rocks approached the Earth surface during exhumation. The temperature at the maximum σ_{twin} is unknown, but is likely to have been less than 170 °C (Ferrill et al., 2004).

(2) The critical resolved shear stress for calcite twinning is generally accepted to be 10 MPa (e.g., Jamison and Spang, 1976; Burkhard, 1993; Lacombe and Laurent, 1996; Lacombe, 2007; and many references therein). If we accept this value and the assumption that it is independent of temperature, a differential stress of at least 20 MPa is required to drive calcite twinning regardless of temperature. Because Type III and Type IV twins are absent in the Syros samples, the magnitude of differential stress in the D–D plastic regime should be less than 20 MPa (Fig. 13). The values of differential stress obtained by the microboudin method are less than 12 MPa (Fig. 9), consistent with the types of calcite twins present in the samples.

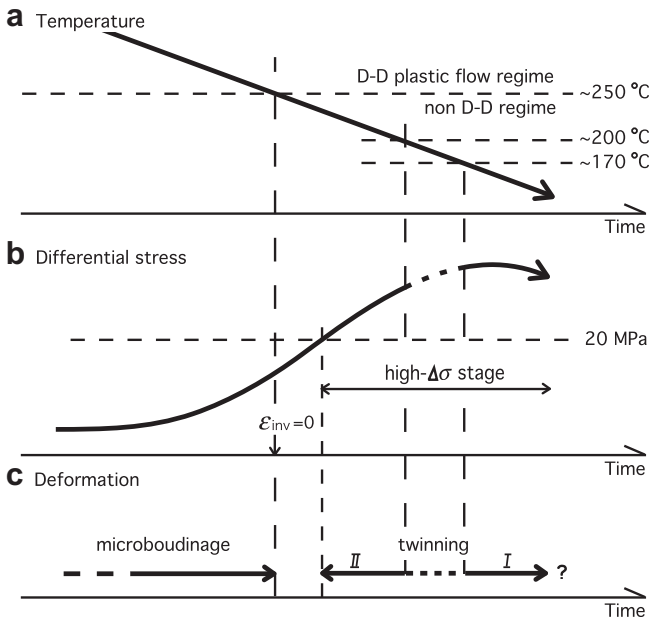

Fig. 13. Temporal trends in temperature, differential stress, and deformation features determined for the analysed samples. (a) Temperature gradually decreased over time. Plastic deformation accommodated by diffusion and dislocation was dominant at about 250 °C (e.g., Passchier and Trouw, 2005), whereas diffusion and dislocation are ineffective in the deformation of calcite at temperatures below about 250 °C (designated as the non D–D regime). (b) A high-$\Delta\sigma$ stage is proposed after the cessation of D–D plastic flow of calcite. The critical differential stress above which calcite twinning actively develops is 20 MPa. (c) Timing of microboudinage and calcite twinning. Microboudinage ceased at $\varepsilon_{inv} = 0$ when the temperature was about 250 °C. Calcite twinning occurred intensively during the high-$\Delta\sigma$ stage. *I*: Type I twinning; *II*: Type II twinning. Thin twins (Type I) are expected to form at <170 °C, while thick twins (Type II) are expected to form at >170 °C (Ferrill et al., 2004). Differential stress at higher temperatures (>250 °C) is expected to be less than 20 MPa (the critical resolved shear stress for calcite twinning is assumed to be independent of temperature), because no calcite twinning occurred at these temperatures. A time lag is expected between the cessation of microboudinage and the initiation of calcite twinning.

(3) From the scheme shown above, differential stress at $\varepsilon_{inv} = 0$ should be less than 20 MPa. This deduction can be used to evaluate the value of K_0/K_c in Eq. (1) of the microboudinage technique. If we treat K_0/K_c as an unknown parameter, it should be less than 0.16, unless the estimated σ_0 becomes larger than 20 MPa at $\varepsilon_{inv} = 0$. Our earlier assumption ($K_0/K_c = 0.1$) is therefore consistent with the calcite-twin data.
(4) There exists a time lag between the cessation of D–D plastic flow of calcite and the initiation of calcite twinning, as shown in Fig. 13.
(5) The method of grain-size palaeopiezometer developed by Schmid et al. (1980) and Rutter (1995) provides three different values of palaeodifferential stress: σ_{SPB}, $\sigma_{R,M}$, and $\sigma_{R,R}$, as shown in Fig. 9. As we have no reliable additional data for determining the mechanism of dynamic recrystallisation in the Syros samples, we cannot judge which value among the three is most appropriate.
(6) Assuming that differential stress estimated using grain-size palaeopiezometry is an average-like representative differential stress that the rocks experienced over the entire history of D–D plastic deformation, σ_{SPB} appears more compatible with σ_0 than do $\sigma_{R,M}$ and $\sigma_{R,R}$, as shown in Fig. 9.

8. Summary

We performed differential stress analyses, using three different methods (microboudin, grain-size, and calcite-twin methods), on two impure marble tectonites collected from Syros, Greece, and obtained the following conclusions.

(1) The microboudin method was successfully applied to impure marbles. Estimates of differential stress obtained using this method are consistent with the critical resolved shear stress estimated from calcite twinning.
(2) The magnitude of differential stress was much higher during calcite twinning than during microboudinage.
(3) Calcite twinning occurred after microboudinage had ceased, during exhumation.
(4) We were unable to select an appropriate grain-size palaeopiezometer for the present analysis.
(5) The palaeodifferential stresses estimated using the three methods are apparently incongruent; however, the microboudin method and the calcite-twin method may in fact be compatible when considering the timing of the differential stress (in terms of the deformation history) recorded by each method.

Acknowledgements

The authors thank K. Sakaguchi for showing us the marble sample containing microboudinaged glaucophane grains, which encouraged this study, and H. Mori for help in the preparation of thin sections. The authors also thank G. E. Lloyd and J. L. Sim for their constructive comments, which led to improvements in the manuscript. This study was financially supported by a grant from the Japanese Society for the Promotion of Science (No. 12354005 awarded to TM).

References

Altherr, R., Kreuzer, H., Wendt, I., Lenz, H., Wagner, G.A., Keller, J., Harre, W., Höhndorf, A., 1982. A late Oligocene/early Miocene high temperature belt in the Cycladic crystalline complex (SE Pelagonian, Greece). Geologisches Jahrbuch E23, 97–164.
Avigad, D., Garfunkel, Z., 1991. Uplift and exhumation of high-pressure metamorphic rocks: the example of the Cycladic blueschist belt (Aegean Sea). Tectonophysics 188, 357–372.
Avigad, D., Garfunkel, Z., Jolivet, L., Azañón, J.M., 1997. Back arc extension and denudation of Mediterranean eclogites. Tectonics 16, 924–941.
Baldwin, S.L., 1996. Contrasting P-T-t histories for blueschists from the western Baja terrane and the Aegean; effects of synsubduction exhumation and backarc extension. In: Bebout, G.E., Scholl, D.W., Kirby, S.H., Platt, J.P. (Eds.), Subduction Top to Bottom. Geophysical Monograph, vol. 96. American Geophysical Union, pp. 135–141.
Bröcker, M., Enders, M., 1999. U–Pb zircon geochronology of unusual eclogite-facies rocks from Syros and Tinos (Cyclades, Greece). Geological Magazine 136, 111–118.
Burkhard, M., 1993. Calcite twins, their geometry, appearance and significance as stress-strain markers and indicators of tectonic regime: a review. Journal of Structural Geology 15, 351–368.
De Bresser, J.H.P., Evans, B., Renner, J., 2002. On estimating the strength of calcite rocks under natural conditions. In: De Meer, S., Drury, M.R., De Bresser, J.H.P., Pennock, G.M. (Eds.), Deformation Mechanisms, Rheology and Tectonics: Current Status and Future Perspective. Geological Society of London, Special Publication, vol. 200, pp. 309–329.
Dixon, J.E., Ridley, J., 1987. Syros. In: Helgeson, H.C. (Ed.), Chemical Transport in Metasomatic Processes. Reidel Publishing Company, Dordrecht, pp. 489–501.
Dixon, J.E., 1976. Glaucophane schists of Syros, Greece. Bulletin de la Societe Géologique de France 7, 280.
Etheridge, M.A., Wilkie, J.C., 1981. An assessment of dynamically recrystallized grainsize as a paleopiezometer in quartz-bearing mylonite zones. Tectonophysics 78, 475–508.
Ferguson, C.C., Lloyd, G.E., 1982. Palaeostress and strain estimates from boudinage structure and their bearing on the evolution of a major Variscan fold-thrust complex in Southwest England. Tectonophysics 88, 269–289.
Ferguson, C.C., Lloyd, G.E., 1984. Extension analysis of stretched belemnites: a comparison of methods. Tectonophysics 101, 199–206.
Ferguson, C.C., 1981. A strain reversal method for estimating extension from fragmented rigid inclusions. Tectonophysics 79, T43–T52.
Ferguson, C.C., 1985. Spatial analysis of extension fracture systems: a process modelling approach. Mathematical Geology 17, 403–425.

Ferguson, C.C., 1987. Fracture and separation histories of stretched belemnites and other rigid-brittle inclusions in tectonites. Tectonophysics 139, 255–273.
Ferrill, D.A., Morris, A.P., Evans, M.A., Burkhard, M., Groshong Jr., R.H., Onasch, C.M., 2004. Calcite twin morphology: a low-temperature deformation geothermometer. Journal of Structural Geology 26, 1521–1529.
Ferrill, D.A., 1998. Critical re-evaluation of differential stress estimates from calcite twins in coarse-grained limestones. Tectonophysics 285, 77–86.
Forster, M.A., Lister, G.S., 2005. Several distinct tectono-metamorphic slices in the Cycladic eclogite-blueschist belt, Greece. Contributions to Mineralogy and Petrology 150, 523–545.
Goscombe, B.D., Passchier, C.E., Hand, M., 2004. Boudinage classification: end-member boudin types and modified boudin structures. Journal of Structural Geology 26, 739–763.
Jamison, W.R., Spang, J.H., 1976. Use of calcite twin lamellae to infer differential stresses. Geological Society of America Bulletin 87, 868–872.
Kimura, N., Awaji, H., Okamoto, M., Matsumura, Y., Masuda, T., 2006. Fracture strength of tourmaline and epidote by three-point bending test: application to microboudin method for estimating absolute magnitude of palaeodifferential stress. Journal of Structural Geology 28, 1093–1102.
Kimura, N., Nakayama, S., Tsukimura, K., Miwa, S., Okamoto, A., Masuda, T., 2010. Determination of amphibole fracture strength for quantitative palaeostress analysis using microboudinage structures. Journal of Structural Geology 32, 136–150.
Kohlstead, D.L., Weathers, M.S., 1980. Deformation-induced microstructures, paleopiezometers and differential stress in deeply eroded fault zones. Journal of Geophysical Research 85, 6269–6285.
Lacombe, O., Laurent, P., 1992. Determination of principal stress magnitudes using calcite twins and rock mechanics data. Tectonophysics 202, 83–93.
Lacombe, O., Laurent, P., 1996. Determination of deviatoric stress tensors based on inversion of calcite twin data from experimentally deformed monophase samples: preliminary results. Tectonophysics 255, 188–202.
Lacombe, O., 2007. Comparison of paleostress magnitudes from calcite twins with contemporary stress magnitudes and frictional sliding criteria in the continental crust: mechanical implications. Journal of Structural Geology 29, 86–99.
Laurent, P., Tourneret, C., Lacombe, O., 1990. Determining deviatoric stress tensors from calcite twins: application to monophase synthetic and natural polycrystals. Tectonics 9, 379–389.
Lister, G.S., Banga, G., Feenstra, A., 1984. Metamorphic core complex of Cordilleran type in the Cyclades, Aegean Sea, Greece. Geology 12, 221–225.
Lloyd, G.E., Condliffe, E., 2003. 'Strain Reversal': a Windows™ program to determine extensional strain from rigid-brittle layers of inclusions. Journal of Structural Geology 25, 1141–1145.
Lloyd, G.E., Ferguson, C.C., Reading, K., 1982. A stress transfer model for the development of extension fracture boudinage. Journal of Structural Geology 4, 355–372.
Maluski, H., Bonneau, M., Kienast, J.R., 1987. Dating the metamorphic events in the Cycladic area: $^{40}Ar/^{39}Ar$ data from metamorphic rocks of the island of Syros (Greece). Bulletin de la Societe Géologique de France 8, 833–842.
Masuda, T., Shibutani, T., Igarashi, T., Kuriyama, M., 1989. Microboudin structure of piedmontite in quartz schists: a proposal for a new indicator of relative palaeodifferential stress. Tectonophysics 163, 169–180.
Masuda, T., Shibutani, T., Kuriyama, M., Igarashi, T., 1990. Development of microboudinage: an estimate of changing differential stress with increasing strain. Tectonophysics 178, 379–387.
Masuda, T., Shibutani, T., Morikawa, T., Ohurasaka, K., Nam, T.N., 1994. Geoscience Reports of Shizuoka University. Calculation of Extension Strain from Boudin Structure: A Computer Program, vol. 20. http://ir.lib.shizuoka.ac.jp/handle/10297/326, pp. 203–208. (in Japanese with English abstract).
Masuda, T., Kugimiya, Y., Aoshima, I., Hara, Y., Ikei, H., 1999. A statistical approach to determination of a mineral lineation. Journal of Structural Geology 21, 467–472.
Masuda, T., Kimura, N., Hara, Y., 2003. Progress in microboudin method for palaeostress analysis of metamorphic tectonites: application of mathematically refined expression. Tectonophysics 364, 1–8.
Masuda, T., Nakayama, S., Kimura, N., Onodera, K., Okamoto, A., 2004. Triaxial stress state deep in orogenic belts: an example from Turkey. Journal of Structural Geology 26, 2203–2209.
Masuda, T., Kimura, N., Okamoto, A., Miyake, T., Omori, Y., 2007. Cessation of plastic deformation during exhumation of metamorphic tectonites revealed by microboudinage structures. Journal of Structural Geology 29, 159–165.
Masuda, T., Nakayama, S., Kimura, N., Okamoto, A., 2008. Magnitude of σ_1, σ_2, and σ_3 at mid-crustal levels in an orogenic belt: microboudin method applied to an impure metachert from Turkey. Tectonophysics 460, 230–236.
Mercier, J.-C.C., Anderson, D.A., Carter, N.L., 1977. Stress in the lithosphere: inferences from steady state flow of rocks. Pure and Applied Geophysics 115, 199–226.
Mercier, J.-C.C., 1980. Magnitude of continental lithospheric stress inferred from rheomorphic petrology. Journal of Geophysical Research 85, 6293–6303.
Misch, P., 1969. Paracrystalline microboudinage of zoned grains and other criteria for synkinematic growth of metamorphic minerals. American Journal of Science 267, 43–63.
Misch, P., 1970. Paracrystalline microboudinage in a metamorphic reaction sequence. Geological Society of America Bulletin 81, 2483–2486.
Okamoto, A., Miyake, T., Masuda, T., 2006. Reaction progress related to indentation structures at glaucophane/glaucophane contacts in an impure marble from Syros, Greece. Journal of Metamorphic Geology 24, 703–713.
Okrusch, M., Bröcker, M., 1990. Eclogites associated with high-grade blueschists in the Cycladic archipelago, Greece: a review. European Journal of Mineralogy 2, 451–478.
Ord, A., Christie, J.M., 1984. Flow stress from microstructures in mylonitic quartzites of the Moine thrust zone, Assynt area, Scotland. Journal of Structural Geology 6, 639–654.
Passchier, C.W., Trouw, R.A.J., 2005. Microtectonics, second ed.. Springer, Berlin.
Pfiffner, O.A., 1982. Deformation mechanisms and flow regimes in limestones from the Helvetic zones of the Swiss Alps. Journal of Structural Geology 4, 429–444.
Rowe, K.J., Rutter, E.H., 1990. Paleostress estimation using calcite twinning: experimental calibration and application to nature. Journal of Structural Geology 12, 1–17.
Rutter, E.H., 1995. Experimental study of the influence of stress, temperature, and strain on the dynamic recrystallization of Carrara marble. Journal of Geophysical Research 100, 24651–24663.
Schmid, S.M., Paterson, M.S., Boland, J.N., 1980. High temperature flow and dynamic recrystallization in Carrara marble. Tectonophysics 65, 245–280.
Sellars, C.M., 1978. Recrystallization of metals during hot deformation. Philosophical Transactions of the Royal Society of London A 288, 147–158.
Shimizu, I., 2008. Theories and applicability of grain size piezometers: the role of dynamic recrystallization mechanisms. Journal of Structural Geology 30, 899–917.
Simmons, G., Wang, H., 1971. Single Crystal Elastic Constants and Calculated Aggregate Properties: A Handbook. MIT Press, Cambridge.
Tomaschek, F., Kennedy, A.K., Villa, I.M., Lagos, M., Ballhaus, C., 2003. Zircons from Syros, Cyclades, Greece: recrystallization and mobilization of zircon during high-pressure metamorphism. Journal of Petrology 44, 1977–2002.
Trotet, F., Vidal, O., Jolivet, L., 2001. Exhumation of Syros and Sifnos metamorphic rocks (Cyclades, Greece): new constraints on the P-T paths. European Journal of Mineralogy 13, 901–920.
Turner, F.J., 1953. Nature and dynamic interpretation of deformation lamellae in calcite of three marbles. American Journal of Science 251, 276–298.
Twiss, R.J., 1977. Theory and applicability of a recrystallized grain size palaeopiezometer. Pure and Applied Geophysics 115, 227–244.
van der Pluijm, B., Marshak, S., 2004. Earth Structure, second ed.. W. W. Norton & Company, London.
Weibull, W., 1951. A statistical distribution function of wide applicability. Journal of Applied Mechanics 22, 293–297.
Zhao, P., Ji, S., 1997. Refinements of shear-lag model and its applications. Tectonophysics 279, 37–53.